Available online at www.sciencedirect.com
SCIENCE DIRECT®
Applied Mathematical Modelling 30 (2006) 1406–1427
APPLIED MATHEMATICAL MODELLING
www.elsevier.com/locate/apm

3D SPH flow predictions and validation for high pressure die casting of automotive components

P.W. Cleary [a], J. Ha [a,*], M. Prakash [a], T. Nguyen [b]

[a] *CSIRO Mathematical and Information Sciences, CRC for Cast Metals Manufacturing (CAST), Private Bag 10, Gate 7, Clayton South MDC, 71 Normany Road, VIC 3169, Australia*
[b] *CSIRO Manufacturing and Infrastructure Technology, Preston, VIC 3072, Australia*

Received 3 August 2004; accepted 13 November 2005
Available online 24 April 2006

Abstract

The geometric complexity and high fluid speeds involved in high pressure die casting (HPDC) combine to give strongly three-dimensional fluid flow with significant free surface fragmentation and splashing. A Lagrangian simulation technique that is particularly well suited to modelling HPDC is smoothed particle hydrodynamics (SPH). Materials are approximated by particles that are free to move around rather than by fixed grids, enabling the accurate prediction of fluid flows involving complex free surface motion.

Validation of isothermal SPH flow predictions for the casting of a servo piston head using water analogue experiments is presented. Comparison with MAGMAsoft predictions provides information of the relative strengths of these two approaches. The SPH simulations were better able to capture the key details of the fluid motion and splashing, particularly the relative rates of flow around sharp bends and through thin sections. Validation of flow predictions coupled to temperature and solidification using short shots are also presented. The bulk features of the final solid castings are in good agreement with the predictions.

Several automotive examples of SPH simulated HPDC flows are presented, ranging from simple cases such as a servo piston to steering column components and a full engine rocker cover. These show unprecedented detail in the fluid free surfaces, particularly in the extent of fragmentation and void formation.

These results together combine to demonstrate that SPH modelling of HPDC has now reached a level where both isothermal and thermal simulations can be performed in reasonable computation times for large scale automotive castings and provide a high degree of predictive accuracy.

Keywords: SPH; High pressure die casting; Automotive components; Water analog model

* Corresponding author. Tel.: +61 3 9545 8004; fax: +61 3 9545 8080.
E-mail address: Joseph.Ha@csiro.au (J. Ha).

0307-904X/$ - see front matter
doi:10.1016/j.apm.2006.03.012

1. Introduction

High pressure die casting (HPDC) is an important process in the manufacturing of high volume and low cost automotive components, such as automatic transmission housings and gear box components. Liquid metal (generally aluminium) is injected into the die at high speed (30–100 m/s) and under high pressure through complex gate and runner systems. The geometric complexity of the dies lead to strongly three-dimensional fluid flow with significant free surface fragmentation and splashing. The order in which the various parts of the die fill and the positioning of the air vents are crucial to forming homogeneous cast components with minimal entrapped voids. This is influenced by the design of the gating system and the geometry of the die. Numerical simulation offers a powerful and cost effective way to study the effectiveness of different die designs and filling processes, ultimately leading to improvements to both product quality and process productivity, including more effective control of the die filling and die thermal performance.

A popular commercially available software package for casting simulations and analysis is MAGMAsoft [1]. It is grid based and employs the volume-of-fluid (VOF) method for tracking interfaces. A simulation technique that has the potential to further improve the level of modelling of HPDC is SPH (see [2] for a review of the method). It is a Lagrangian (grid-free) method for modelling heat and mass flows and is well suited to simulating free surface flows of the present kind. For examples of its application see Monaghan et al. [3] for simulation of gravity currents on a ramp and Monaghan and Kos [4] and Monaghan and Kos [5] for simulation of the Scott Russell's wave generator.

In SPH, materials are approximated by particles that are free to move around rather than by fixed grids or meshes. The particles are basically moving interpolation points that carry with them physical properties, such as the mass of the fluid, its temperature, enthalpy, density and any other properties that are relevant, such as stress and strain history dependent rheology. The inter-particle forces are calculated by smoothing the information from nearby particles in a way that ensures that the resultant particle motion is consistent with the motion of a corresponding real fluid, as determined by the Navier–Stokes equations.

SPH has been developed over the past two decades initially for astrophysical applications [2] and more recently for incompressible enclosed flows [2]. It is also able to model low-speed incompressible flow [6,7], viscous flow [8], underwater explosion [9] and galaxy formation [10]. Examples of other applications include heat conduction [11], natural convection in a cavity and Rayleigh–Benard convective instability [12] and high pressure die casting [13,14]. Examples of validation of simple free surface flows can be found in recent work by Monaghan and co-workers [3–5].

Recently, Cleary et al. [14] and Ha and Cleary [15] reported on the application of SPH to HPDC in two-dimensions and the favourable comparison of these SPH results with water analogue experiments. It should be noted that particularly good resolution of the small scale fluid structures was obtained along with accurate predictions of voids in the flow. Ha et al. [16] compared SPH simulations with water analogue modelling of gravity die casting for a complex die in two different orientations. The SPH simulations were able to capture the free surface wave behaviour and the fine details of the flow.

In this paper, we describe the use of SPH in 3D to predict the filling of several real automotive components and examine the accuracy of the SPH solutions by comparison to water analogue experiments, short shots experiments and MAGMAsoft simulation predictions. This will show that SPH is in fact well suited to simulating such complex industrial flow processes.

2. The SPH method

SPH is a particle based method for modelling coupled fluid flows, solid structure deformation and heat transfer. The particles represent blobs of discretised fluid or solids that move around in response to the fluid or solid stresses produced by the interaction with other particles. Importantly, SPH does not use any fixed grids or meshes to track the fluid and calculate the fluid velocities.

Formally, SPH is a Lagrangian continuum method for solving systems of partial differential equations. The fluid (or solid) is discretised and the properties of each of these fluid/solid elements are attributed to their centers, which are then interpreted as a particles. SPH uses an interpolation kernel to smooth the values of any

information held by the particles to give smooth continuous interpolated fields (e.g. smooth density or pressure fields from the discrete values of fluid density and pressure at the particles).

2.1. SPH interpolation

In SPH, each particle b has properties: mass m_b, position $\boldsymbol{r}_b$, density ρ_b and velocity $\mathbf{v}_b$. The interpolated value of any field A at position $\mathbf{r}$ is approximated using information from these particles by

$$A(\boldsymbol{r}) = \sum_b m_b \frac{A_b}{\rho_b} W(\mathbf{r} - \mathbf{r}_b, h), \tag{1}$$

where W is an interpolating kernel, h is the interpolation length and the value of A at $\mathbf{r}_b$ is denoted by A_b. The sum is over all particles b within a radius $2h$ of $\mathbf{r}_b$. $W(\mathbf{r}, h)$ is a spline based interpolation kernel of radius $2h$. It is a twice differentiable function that approximates the shape of a Gaussian function and has compact support. This allows smoothed approximations to the physical properties of the fluid to be calculated from the particle information. The smoothing formalism also provides a way to find gradients of fluid properties. The gradient of the function A is then given by

$$\nabla A(\boldsymbol{r}) = \sum_b m_b \frac{A_b}{\rho_b} \nabla W(\mathbf{r} - \mathbf{r}_b, h). \tag{2}$$

In this way, the SPH representation of the hydrodynamic governing equations can be built from the Navier–Stokes equations.

2.2. Continuity equation

The SPH continuity equation, taken from Monaghan [2] and Monaghan [17], is

$$\frac{\mathrm{d}\rho_a}{\mathrm{d}t} = \sum_b m_b (\mathbf{v}_a - \mathbf{v}_b) \cdot \nabla W_{ab}. \tag{3}$$

We denote the position vector from particle b to particle a by $\mathbf{r}_{ab} = \mathbf{r}_a - \mathbf{r}_b$ and let $W_{ab} = W(\mathbf{r}_{ab}, h)$ be the interpolation kernel evaluated for the distance $|\mathbf{r}_{ab}|$. This form of the continuity equation is Galilean invariant (since the positions and velocities appear only as differences), has good numerical conservation properties and is not affected by free surfaces or density discontinuities. The use of this form of the continuity equation is very important for predicting free surface flows such as those occurring in various environmental fluid flows.

As two particles approach each other, their relative velocity is negative (as is the gradient of the kernel) so that there is a positive contribution to $\frac{\mathrm{d}\rho_a}{\mathrm{d}t}$. If this rate of change is positive then the density of particle a rises, leading to a positive pressure that pushes the particles apart again. If two particles move apart, then their densities decrease creating a negative pressure that pulls the particles back towards each other. This interplay of velocity and density/pressure ensures that the particle remains 'on average' equally spaced and that the density is close to uniform, so that the fluid is close to incompressible.

2.3. Momentum equation

The SPH momentum equation used is from Cleary [12]:

$$\frac{\mathrm{d}\mathbf{v}_a}{\mathrm{d}t} = -\sum_b m_b \left[\left(\frac{P_b}{\rho_b^2} + \frac{P_a}{\rho_a^2} \right) - \frac{\xi}{\rho_a \rho_b} \frac{4\mu_a \mu_b}{(\mu_a + \mu_b)} \frac{\mathbf{v}_{ab} . \mathbf{r}_{ab}}{\mathbf{r}_{ab}^2 + \eta^2} \right] \nabla_a W_{ab} + \mathbf{g}, \tag{4}$$

where P_a and μ_a are pressure and viscosity of particle a and $\mathbf{v}_{ab} = \mathbf{v}_a - \mathbf{v}_b$. Here η is a small parameter used to smooth out the singularity at $\mathbf{r}_{ab} = 0$ and $\mathbf{g}$ is the gravity vector.

The first two terms involving the pressure correspond to the pressure gradient term of the Navier–Stokes equation. The next term involving viscosities is the Newtonian viscous stress term. This form ensures that stress is automatically continuous across material interfaces and allows the viscosity to be variable or

discontinuous. Multiple materials with viscosities varying by up to five orders of magnitude within a couple of particle spacings can be easily and accurately simulated.

The time step for the explicit integration used in these simulations is limited by the Courant condition modified for the presence of viscosity:

$$\Delta t = \min_a \left\{ 0.5\mathrm{h} \Big/ \left(c_s + 2\xi \frac{\mu_a}{h\rho_a} \right) \right\}, \tag{5}$$

where c_s is the local speed of sound.

2.4. Energy equation

The SPH heat equation is derived from the internal energy equation developed in Cleary and Monaghan [11] by using an enthalpy formulation for solidifying metals (see Cleary et al. [13]):

$$\frac{\mathrm{d}H_a}{\mathrm{d}t} = \sum_b \frac{4m_b}{\rho_a \rho_b} \frac{k_a k_b T_{ab}}{k_a + k_b} \frac{\mathbf{r}_{ab} \cdot \nabla_a W_{ab}}{\mathbf{r}_{ab}^2 + \eta^2}, \tag{6}$$

where the right hand side is for heat conduction and the enthalpy per unit mass is given by

$$H = \int_0^T c_p(\theta)\,\mathrm{d}\theta + L[1 - f_s(T)], \tag{7}$$

where c_p is the temperature dependent specific heat, L is the latent heat and $f_s(T)$ is the volume fraction of metal that is solid at temperature T. k_b is the conductivity and $T_{ab} = T_a - T_b$.

Eq. (6) has an explicit conductivity which can be temperature dependent and ensures that heat flux is automatically continuous across material interfaces, such as between lava and the ground below. This allows multiple materials with substantially different conductivities and specific heats to be accurately simulated. The accuracy of the conduction solutions are demonstrated in Cleary and Monaghan [11].

2.5. Equation of state

SPH is a compressible method which is used near the incompressible limit by choosing a sound speed that is much larger than the velocity scales in the flow. This quasi-incompressible limit is actually what happens with real fluids. The equation of state, giving the relationship between particle density and fluid pressure, is:

$$P = P_0 \left[\left(\frac{\rho}{\rho_0} \right)^{\gamma} - 1 \right], \tag{8}$$

where P_0 is the pressure scale factor and ρ_0 is the reference density. For water or liquid metals the exponent $\gamma = 7$ is used. This pressure is then used in the SPH momentum equation (4) to give the particle motion.

The pressure scale factor P_0 is given by

$$\frac{\gamma P_0}{\rho_0} = 100V^2 = c_s^2, \tag{9}$$

where V is the characteristic or maximum fluid velocity. Essentially, the Mach number is chosen to be 0.1. This choice maintains effective incompressibility without making the Courant condition too severe. Also, this ensures that the density variation is less than 1% and the flow can be regarded as incompressible.

2.5.1. Boundaries

Boundaries in SPH can be modelled in a range of ways, but here we use approximately evenly spaced stationary SPH particles at which a Lennard-Jones type force (a very steep polynomial variation of force with displacement) is applied in the normal direction. The boundary particles are included in the calculations of the viscous stress using Eq. (9) (with the pressure gradient term set to zero) to produce a non-slip boundary

condition for the fluid. Boundary particles are created by generating triangular meshes of the topographic surfaces from digital terrain models (DTM) in the same way as is done for the discrete element method (DEM), except that the mesh structure is not used, only the nodes (which become particles).

The simulation progresses by explicitly integrating the system of ordinary differential equations (3) and (4) and any secondary equations such as the energy equation. SPH simulations can now be computationally large, from 100,000 to 3 million particles on moderate speed single processor workstations. They can be performed for very complex boundary geometries taken from either CAD surface descriptions. The fluid flow and solid deformation is often coupled to important other physics, such as heat transfer, solidification, curing, phase change and flow in porous media.

3. Validation of isothermal flow

In order to evaluate the accuracy of the SPH predictions of HPDC we compare them to a water analogue experiment and to a MAGMAsoft simulation for the filling of a single servo piston. The automotive component used in this study was as shown in Fig. 9.

3.1. Experimental configuration

In the actual manufacturing process of the servo pistons, a set of 4 pistons are cast at a time (refer to Fig. 9). The filling predictions for this full system are presented below (see Fig. 10). Here, only one servo piston is employed in the die configuration used in our numerical and water-analog modelling of the die filling process.

Fig. 1 shows the schematic of the experimental set-up for the water analog equipment and the image capturing by high speed video camera. The flow of water into the die is controlled by the valve in the pipe joining the vessel and the perspex die. The opening and closing of the valve is carried out by hand. The flow rate is controlled by the pressure in the vessel. The manner of operation means that the flow rate is not well characterised and the fill time estimation has a reasonable range of uncertainty. This makes detailed comparison with either MAGMAsoft or SPH more difficult. In all the simulations presented in this paper, an average flow rate of 1.5 l per second is used.

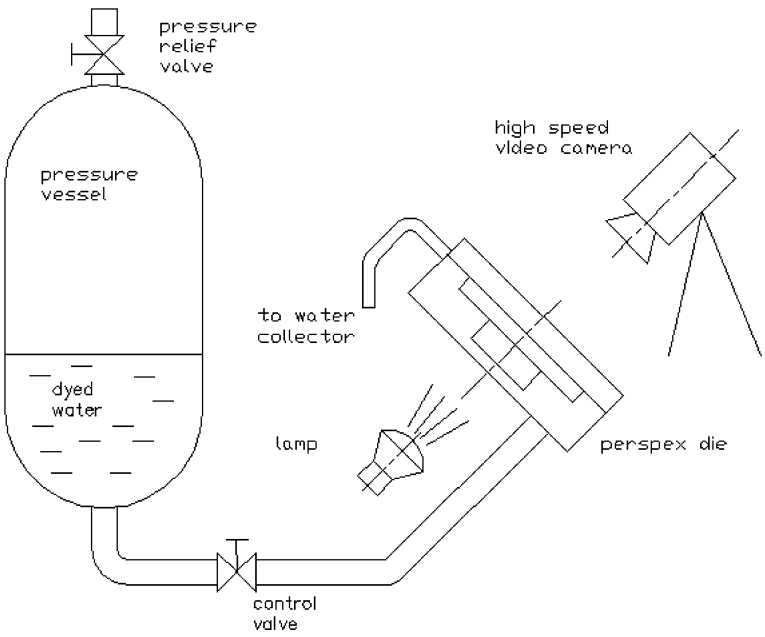

Fig. 1. Experimental set-up for water analog experiment.

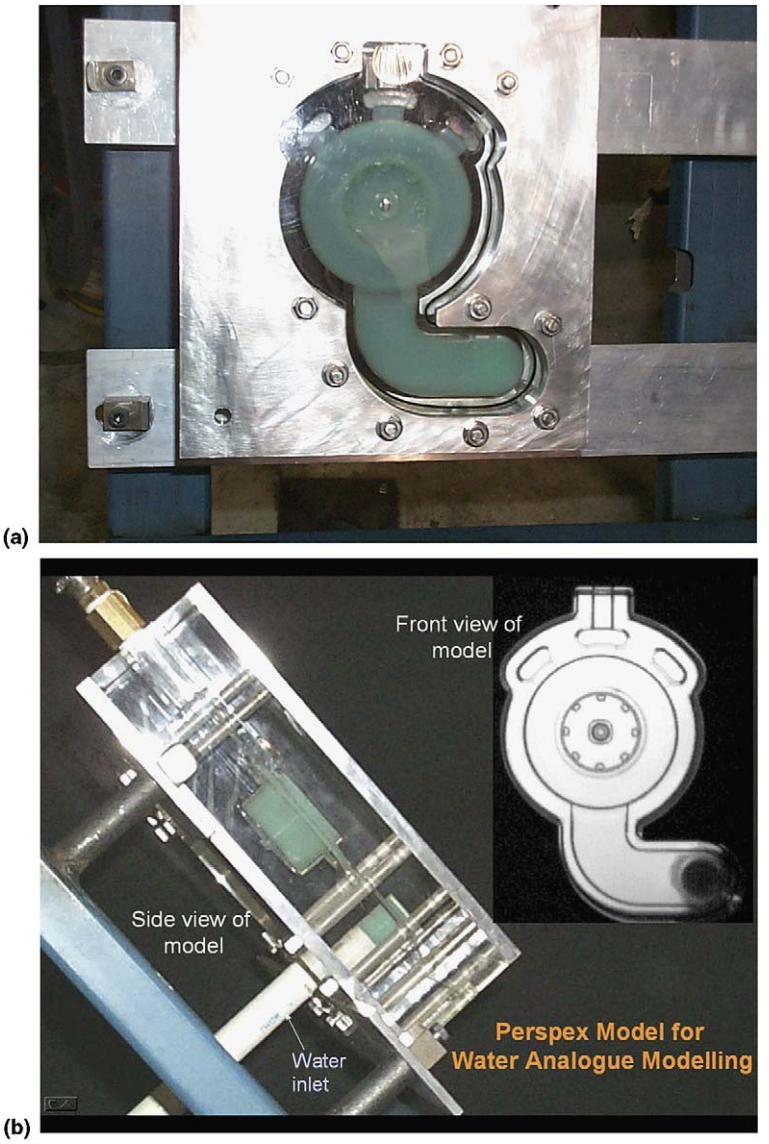

Fig. 2. Perspex model of the die as viewed by the camera (a) and viewed from the side (b). Insert shows an image captured by the camera.

The filling process is captured by a high speed video camera, operating at a shutter speed of 1/20,000 s. Fig. 2a shows the view of the die as seen by the camera. An example of the images captured by the camera is shown in the insert of Fig. 2b. In both figures, the die is shown filled with coloured water.

The water analogue experiment is difficult to perform due to a number of factors. These relate to the capture of images by a high speed video camera, lighting restrictions, the entrainment of air in the high speed fluid flow and the generation of bubbles in the water during flow through the shot sleeve. This means the images captured are not as clear and definitive as one might like and any obstruction that affects the transmission of light to the camera appears as some shade of grey.

3.2. The simulations

In both the SPH and MAGMAsoft simulations, the filling processes were assumed to be isothermal and the fluid properties (density and viscosity at the temperature of 20 °C) used were those of water. No surface

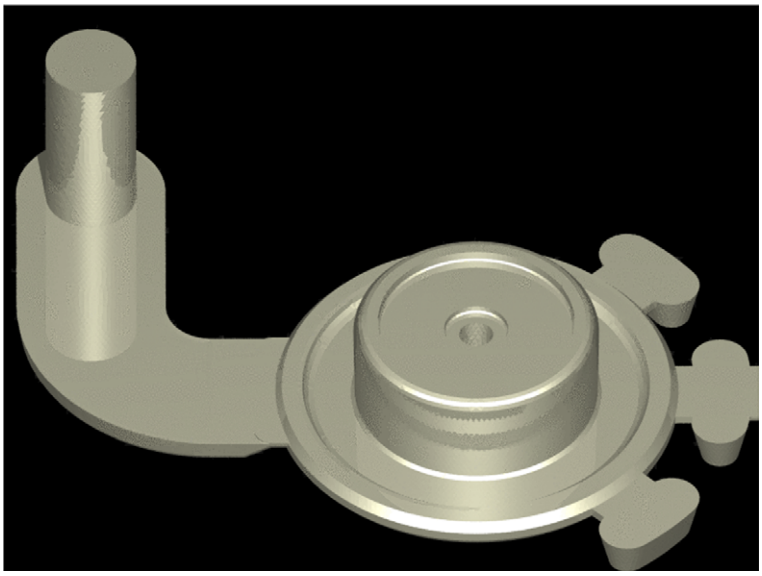

Fig. 3. Geometry of die used for the experiment and numerical simulations.

tension or turbulence models were included in either form of simulation. Both the SPH and MAGMAsoft simulations were performed in 3D. Fig. 3 shows the geometry of die used for numerical simulations.

In the SPH simulations, a particle spacing of 1.44 mm was used. Test runs at coarser and finer resolutions showed little difference in the results. Note that the gate height of the system is 3.0 mm. To simulate the inlet boundary condition, particles were periodically generated at the inlet of the pipe and moved upward with the specified inlet velocity creating a flow of regularly spaced particles travelling up towards the runner. The number of particles in the simulation therefore increases steadily with time. When full, the SPH solution has 50,000 particles.

For comparison with the experiment, the SPH particles were depth averaged and the shading made proportional to the fluid depth in order to mimic the shading effect captured by the camera. This was found to be the fairest representation of the simulation that could be produced for a reasonable comparison with the experimental results.

MAGMAsoft [1] is a 3D solidification and fluid flow package used in the die casting industry to model the molten metal flow and solidification in dies. MAGMAsoft employs the finite difference method to solve the heat and mass transfer on a rectangular grid. It can be a useful tool for simulating some molten metal flow but also has some limitations. In particular, the rectangular grid introduces stairstep artifacts along curved and sloping boundaries (see Fig. 4) and the VOF formulation for following the free surfaces is diffusive and leads to mass conservation problems for small fragments and surface features [16].

The die geometry used for the MAGMAsoft simulation was exactly the same as that for SPH simulation. The grid used contained 3,373,812 elements or control volumes. A constant flow rate was set at the inlet. The visualisation of MAGMAsoft results was done by shading the elements according to their velocity.

3.3. Comparison of SPH with experiment and MAGMAsoft

In Fig. 4, the results of SPH and MAGMAsoft simulations at selected stages of filling are compared with results obtained from the water analogue experiment. A degree of caution is required when interpreting the results. In the experimental images, the flow features are necessarily somewhat blurred due to the 1/20,000 frame exposure time. This is because a drop of fluid moving at say 20 m/s makes a 1 mm long streak during the period of frame exposure. For a part of around 110 mm this introduces errors of the order of 1% for the fluid position and blurs the image slightly. On the other hand, SPH draws precise volumes for the fluid particles whilst MAGMAsoft shows the smoothed projected volume of fluid which can appear more solid than it actually is.

In the first frame (at 35 ms) fluid has just started entering the die in all three cases. To maximise the use of camera resolution, only the die itself was imaged so there is no photographic information about the runner part of the flow. In this first frame, the volume of fluid that has entered the die is slightly too large for MAGMAsoft but slightly too small for SPH.

By 40 ms (frame b) the jet of fluid entering the gate has broadened to fill the width of the gate. This wide but thin (in the third dimension) jet then strikes the inside surface of the raised cylindrical section and starts to flow both up and around its sides. This frame shows the widest variance between all three flows. The experimental fluid is very wispy in appearance indicating that the fluid is very fragmented and is blurred by its motion during the frame exposure time. The fluid in the sides of the cylindrical section can be clearly discerned by the solid dark grey between the 5 o'clock and 9 o'clock positions. In the SPH solution, the fluid has not

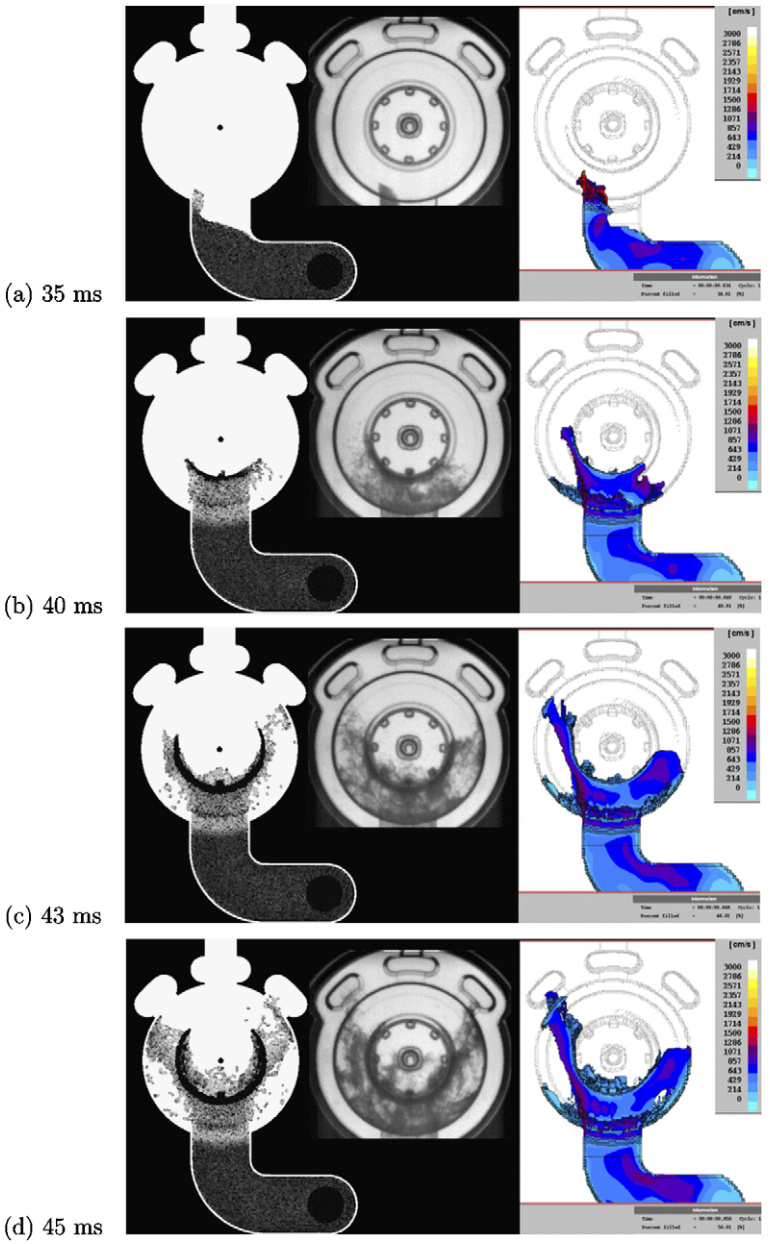

Fig. 4. Comparison between SPH (left), experiment (middle) and MAGMAsoft (right) results at given times.

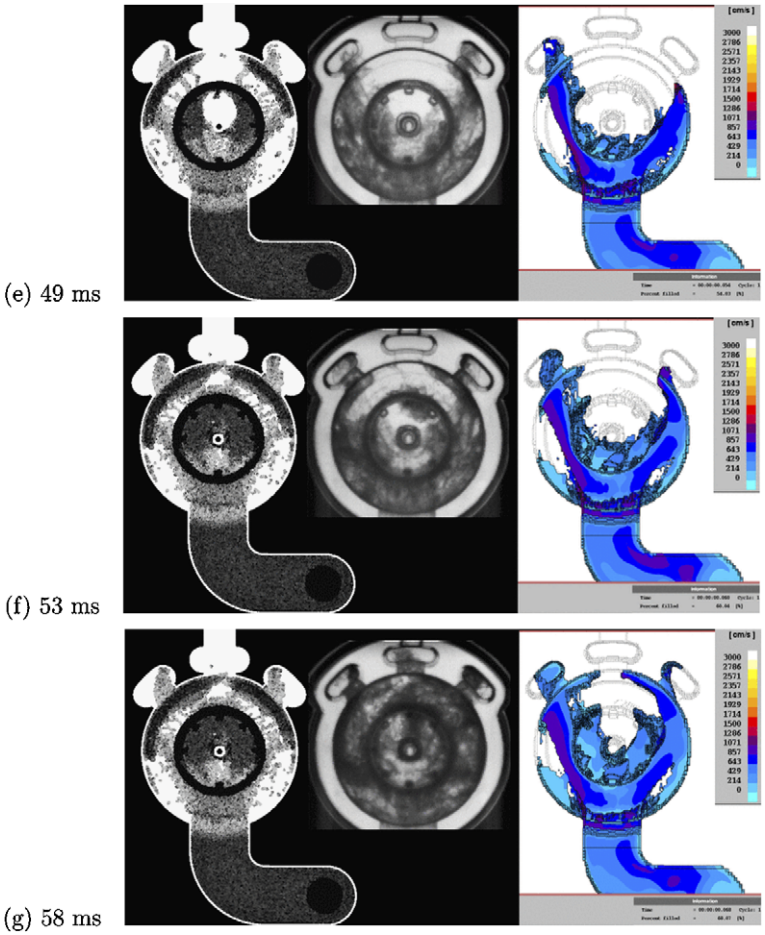

Fig. 4 (*continued*)

been sprayed as widely but remains as a more coherent jet. The SPH prediction for the fluid in the vertical cylindrical section covers about the correct area but is too symmetric. This is thought to result from the omission of air in the simulation, which leads to somewhat different filling dynamics in the last part of the runner leading up to the gate.

The MAGMAsoft prediction appears more realistic for this particular time with better predictions of the fluid flow in the cylindrical section and with the filling to the right of the gate. Two important issues with this solution though are the very strong nature of the jet of fluid that has glanced from the left side of the cylindrical central section and also the filling on the outside of the die on the left adjacent to the gate. This later part of the filling was examined in detail and found to be an erroneous reflection from one of the stair-step cells at the base of the central section.

At 43 ms (frame c) there are increasing differences between the MAGMAsoft solution and the experiment, whilst the SPH solution compares progressively more favourably. A key point of comparison are the front locations of the fluid in the vertical side walls of the central cylindrical section. In the experiment, the fluid occupies a region from about 3 o'clock to 9 o'clock. This region can be seen to be substantially filled since the shade of the fluid is very dark. In the same way, the SPH shading (representing the depth of fluid) is also quite dark and the leading edges are in quite similar positions (perhaps a little too advanced on the right). The SPH fluid has now become fragmented and scattered throughout the front half of the horizontal circular base plate in much the same way as the experiment. The leading fragments though are more advanced on the right than on the left which is opposite to that observed in the experiment. This is again thought to be a legacy of the

absence of air in the pressurisation of the runner system, which has led to the leading egde of SPH fluid being directed preferentially to the right instead of to the left.

The MAGMAsoft solution has some important difficulties at this point. It clearly predicts an overly strong primary jet on the left side of the cylindrical central section. This very coherent jet has already reached the left vent well in advance of the experimental flow. There is also an absence of fragmented fluid to the left of the main jet and in advance of the leading solid edge of fluid on the right. In the vertical cylindrical section the fluid occupies a region from 4 o'clock to 10 o'clock. This is the correct amount of area filled, but it is biased to the left side by the overly strong primary jet.

At 45 ms, the contrasts are becoming stronger. The key points of comparison are that the SPH and experimental fluid are just reaching both the left and the right vents and this fluid is moderately fragmented in both. In both cases the fluid fronts in the central vertical section are at 2 o'clock and 10 o'clock and match closely. The amount of fluid that has entered the horizontal top section of the die (in the middle of the pictures) is closely matched and the fraction of die volume in the horizontal base plate behind the leading jets are quite similar. In contrast, the overly strong left jet of the MAGMAsoft solution has now entered the left vent, but the fluid on the right is significantly short of the right vent. The locations of the fronts in the vertical cylindrical sections are now between 3 and 4 o'clock on the right and 10 o'clock on the left. There is insufficient fluid entering the horizontal raised central section of the die and to the left of the primary jet.

At 49 ms, the fronts of fluid in the vertical cylindrical section are just joining in the experiment. The SPH solution correctly predicts this merging. This demonstrates that the SPH solution is predicting the correct fraction of fluid entering the vertical section of the die with the correct velocities. In contrast, the MAGMAsoft solution is still predicting front locations that are around 3 o'clock and 10 o'clock. SPH is also very accurately predicting the size of the circular entrapped void on the top surface of the raised central section. The SPH solution is now indicating moderate flow in the left and right vents and is in very close agreement with the experiment. Conversely, the SPH solution seems to be predicting moderately too much accumulation of fluid around the rim of the base plate in front of the two vents and also moderately too little fluid in the regions of the base plate on either side of the gate. This suggests a slightly too rapid flow of fluid across the horizontal base plate. Our conjecture here is that this results from the absence of air in the SPH solution. The inclusion of air could be expected to produce a moderate back pressure which would slow this fluid a little and delay the rate at which it leaves the front part of the base plate near the gate and the rate at which it acculumates around the vents. The MAGMAsoft solution is now poorly representing the fragmented fluid on the left side of the die

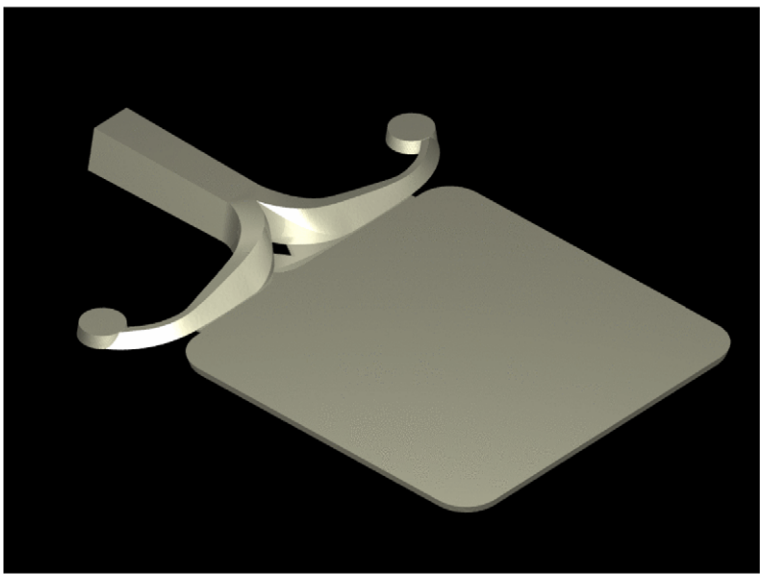

Fig. 5. Geometry of coaster.

to the left of the main jet. Neither does it correctly represent the fluid progress on the right of the die or over the horizontal raised central part of the die.

The same trends previously described continue in the remaining frames. The SPH solution is much closer to the experiment, but both simulations have some erroneous features. The SPH solution continues to have substantially correct predictions for the fraction of the die filled, but with a clear predisposition for the fluid to progress through the die a little too fast leading to a modest over-prediction in the amount of fluid on the vent side of the base plate and a corresponding under-prediction of fluid on the gate side. This is again attributed to

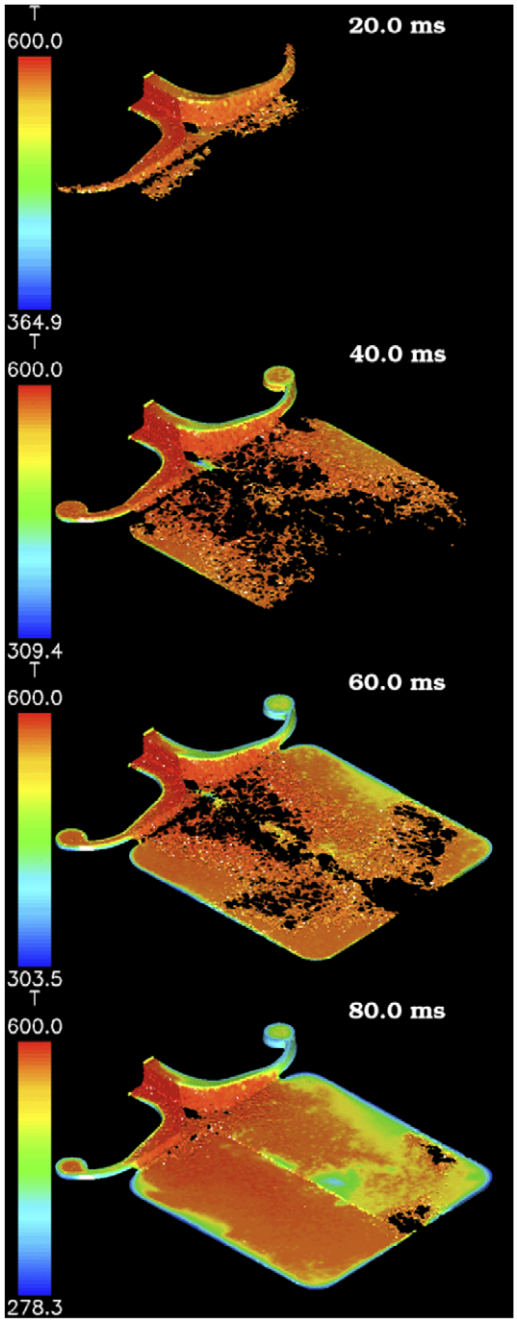

Fig. 6. Filling of coaster with fluid coloured by temperature.

the absence of back pressure due to air, but also due to the absence of entrained gas from both the filling flow and from the shot sleeve. This trapped air in the experiment slows the passage of the fluid from one side of the die to the other. The MAGMAsoft solution continues to have significant errors in key aspects of the flow.

Examining the final frame of the figure, we again see very good agreement between the experiment and the SPH solution, with similar amounts of fluid in the left and right vents, in the horizontal base plate and in the raised central section. Dark bands of fluid are now forming around the rim of the base plate in the experiment as the air is forced out and the fluid fills the full depth of the die. These dark bands in the rim are quite similar

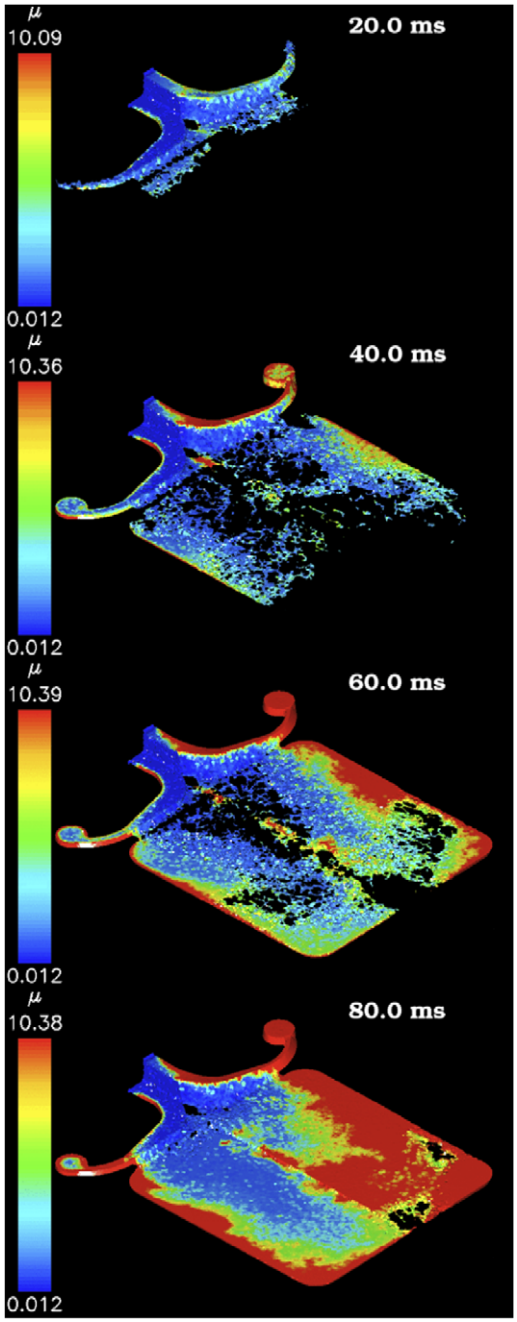

Fig. 7. Filling of coaster with fluid coloured by viscosity.

to the ones observed in the SPH solution. On the negative side, the SPH solution has yet to predict the start of flow through the central vent and is still mildly under-predicting the fraction of fluid filling in the gate half of the base plate.

The MAGMAsoft solution is still exhibiting serious divergences from the experimental flow. The leading edges of fluid on the sides of the vertical cylindrical section have still not met and a reasonable portion of the central horizontal section of the die is yet to be filled. A large section of the base plate opposite the central vent still has no fluid filling it. The leading edges of the fluid moving around the base plate towards the central vent have also not yet made contact. When they do so, there will be an erroneous prediction of a large void region in the base plate directly opposite the central vent due to the unphysically slow flow into this region. Finally, there are reasonable size coherent but unrealistic voids in the base plate on either side of the incoming jet. The SPH solution has also under-predicted the filling in these last regions, but the distribution of fluid is more realistic as is the prediction of the more fragmented nature of that fluid.

Summarising the comparison above, we see that the MAGMAsoft solution is arguably slightly better in the very early stages, but that the SPH solution rapidly overtakes it and is able to make quite accurate predictions for the rates of motion of fluid fronts and the times at which voids are trapped (which will provide good quality predictions of porosity locations). The SPH solution is also able to reasonably accurately capture the

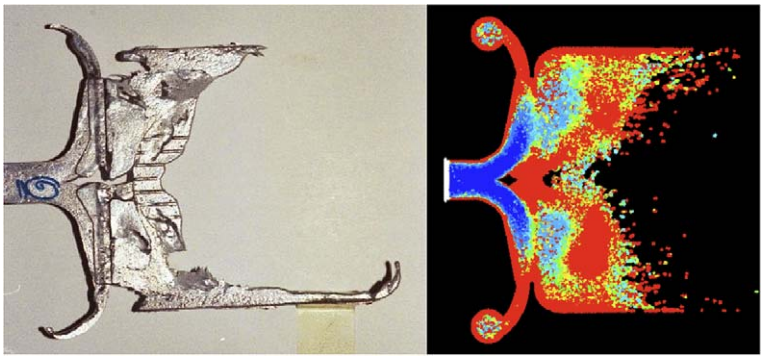

Fig. 8. Short shot: experiment (left), simulation (right).

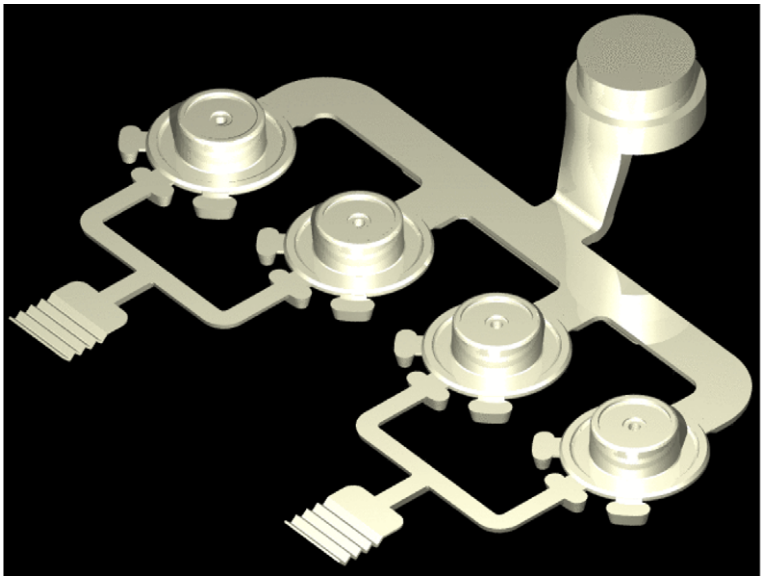

Fig. 9. Geometry of servo piston.

fragmented nature of the fluid flow and many of the finer scale features. The SPH solution though fails to deliver full accuracy with two main discrepancies, both of which can be attributed to the absence of air in the simulation. At the start of the filling, the leading fluid is initially pushed into the die with a slight bias to the right side. This is a legacy of the pattern of filling of the runner in the lead up to the gate. If air were present then this would pressurise in the runner before it was filled and would prevent the sideways flow to the right which fills the runner in the absence of air. This would result in an initial fluid jet path that was directed to the left rather than the right. This explains the early differences in the SPH solution. The second discrepancy is that fluid tends to travel across the base plate a little too fast leading to a modest over-prediction of the fluid build up on the vent side of the base plate and a matching under-prediction on the gate side. This indicates that the presence of air in this particular die filling experiment is moderately important to determining the detailed flow.

For MAGMAsoft, we observe significant quantitative divergences from the experimentally observed flow after the early stages. The key features are the prediction of a significantly too strong jet on the left of the base

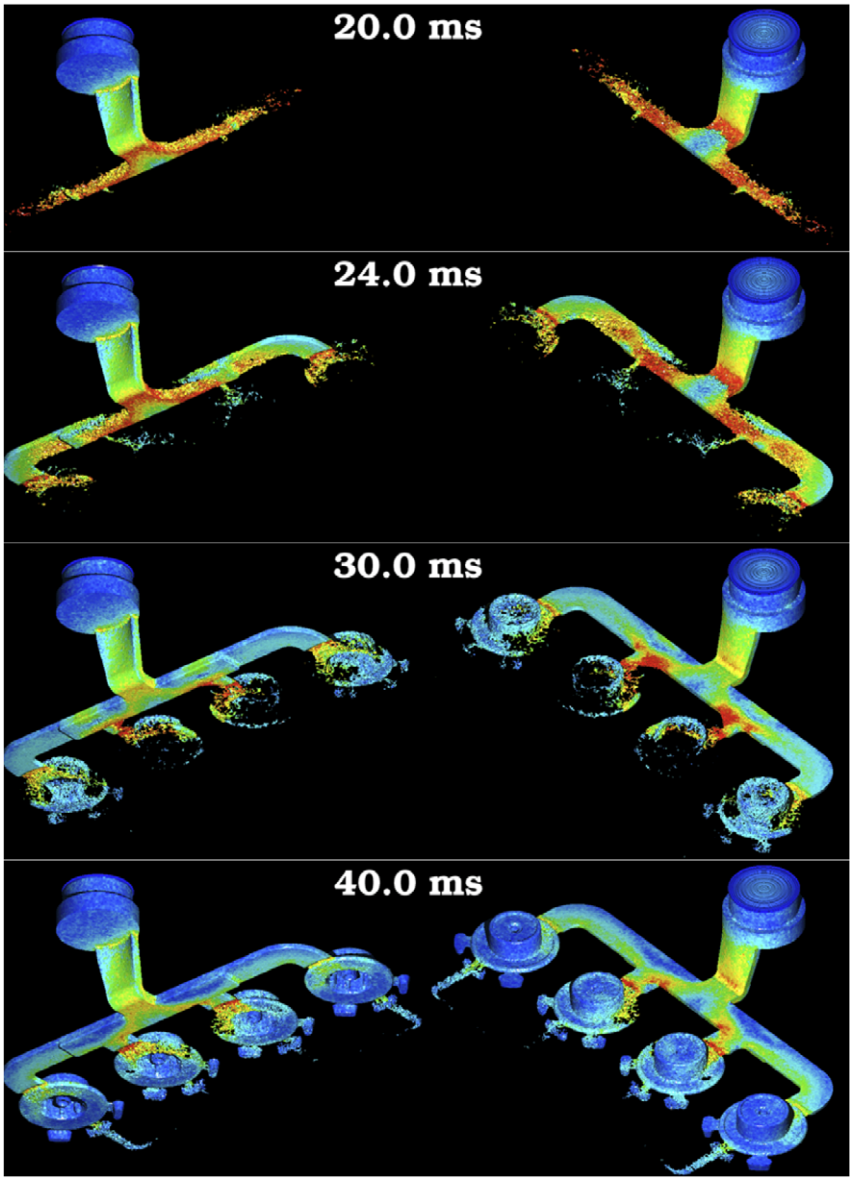

Fig. 10. Filling of servo piston with fluid coloured by velocity.

plate and the substantial under-prediction of fluid entering and the rate of flow around the curved and raised central cylindrical shell. We attribute these problems to the 'stair-step' approximation for the curved surfaces. Since MAGMAsoft uses a regular grid, the curved surfaces are represented by a series of steps as specific grid cells that might or might not be included in the computational domain. These geometry artifacts lead to artificial resistance to flow around curves and bends. This is akin to an additional artificial viscosity in regions of curvature. The size of this resistance decreases with the fineness of the grid used. The grids used for HPDC though are typically quite coarse leading to significant resistance. This preferentially and strongly keeps fluid flowing in the flat horizontal base plate leading to overly strong predictions of the jets on either side of the core. It also leads to significant under prediction of flow into the raised central section and particularly delays the filling around the vertical sides of the raised section. This is likely to result in erroneous deductions of locations of porosity. An important consequence is that the precise details of the porosity predictions will then be potentially quite sensitive to the details of the grid used for a specific simulation. Different grids are likely to lead to changes in the relative strengths of the jets into the various parts of the die leading to mesh/grid dependent predictions.

4. Filling of a simple coaster including solidification

To demonstrate and validate the predictions of the coupled thermal, solidification and flow models, a simple thin square coaster with rounded corners (see Fig. 5) was simulated. Short shot experiments and matching SPH simulations were performed and are compared here.

A tangential runner with a diamond shaped insert in the middle was used. The coaster was 9 cm × 9 cm and 2 mm in thickness. The gate was 0.9 mm thick and a particle size of 0.6 mm was used. The simulation used a fully coupled fluid and heat flow model. Conduction was predicted in both the solidifying liquid metal and into and through the die. Temperature dependent material properties, particularly viscosity and the release of latent heat were included.

4.1. Filling of the coaster with solidifying metal

Figs. 6 and 7 show the fluid temperature and viscosity respectively during the filling. All the fluid is shown on the right side of the die, so the colouring shows the surface properties. On the left only the material in the bottom half of the die is shown. The temperature and viscosity shown on the top left surface therefore belongs to fluid in the mid-plane of the die. Surrounding the fluid shown here is the solid die, but it is not shown. For the coupled thermal flow, heat conduction from the liquid metal into the die is critical to determine the solidification and therefore viscosity of the fluid. This has a major impact on the predicted fill pattern.

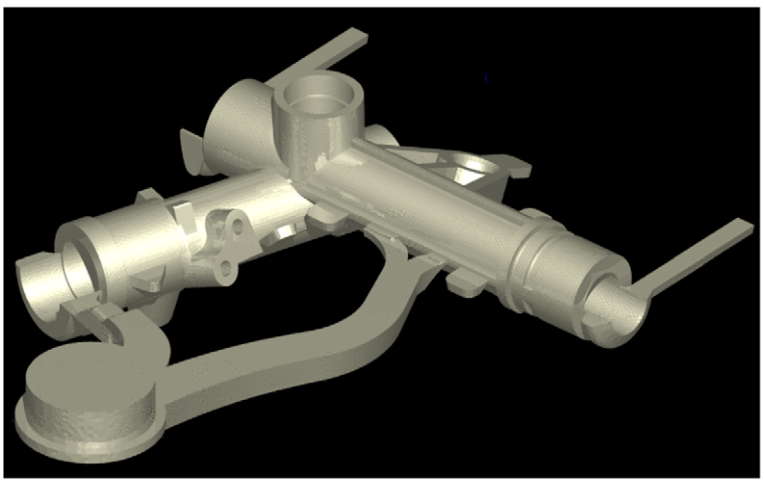

Fig. 11. Geometry of steering column.

Once the tangential runner fills and pressurises, fluid is sprayed out into the die on 45° angled trajectories towards the side walls. Liquid metal builds up along the side walls slowing as it cools and becomes more viscous. Once the metal also makes contact with the colder top and bottom walls of the die, the cooling and solidification accelerate. The central parts of the die cavity are filled with a fairly sparse and highly fragmented hot liquid metal. Along the centreline of the die, splashing liquid metal from either side collide and stick to the top and bottom walls forming a fragmented line of prematurely solid metal. The build up of metal on the sides of the die leads to a back filling flow towards the gate.

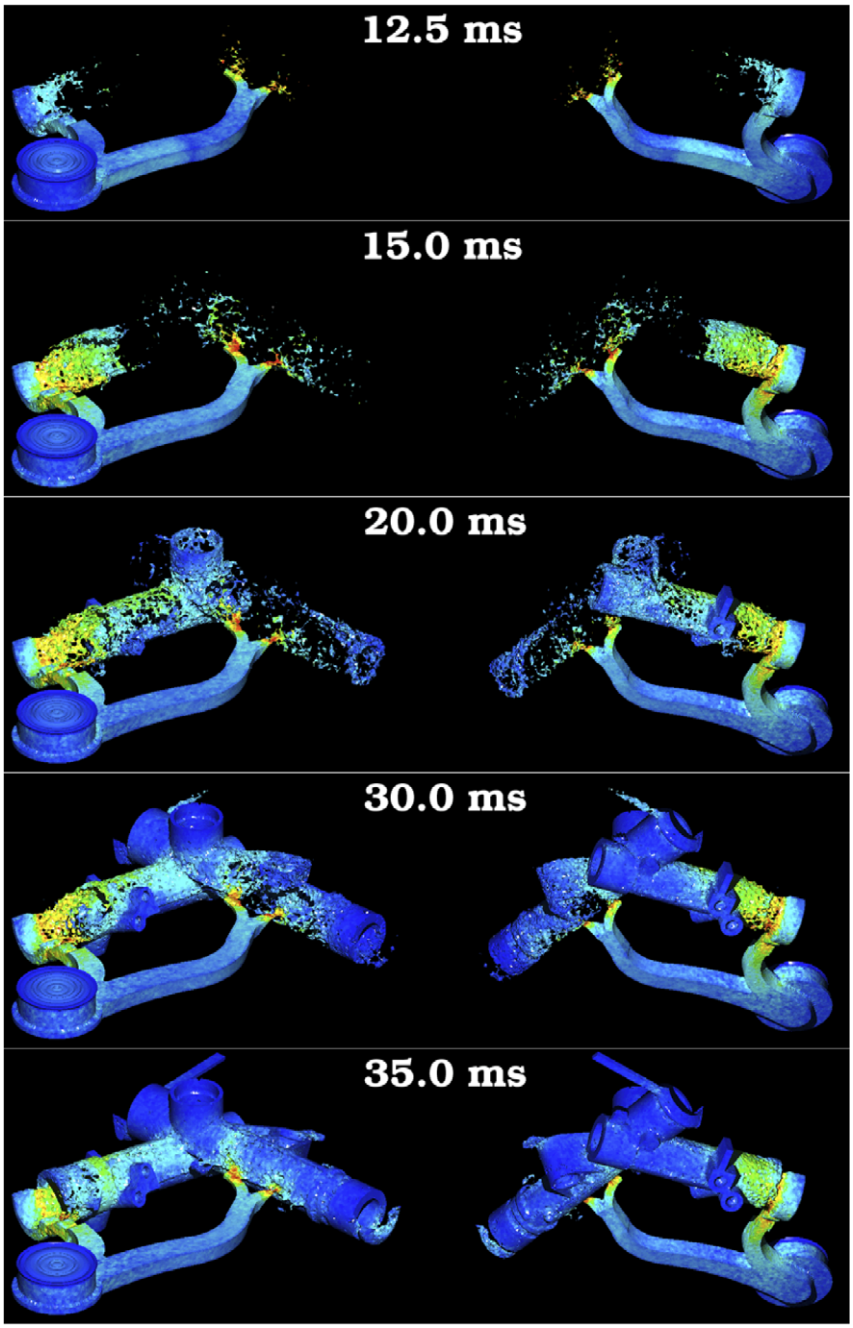

Fig. 12. Filling of steering column with fluid coloured by velocity.

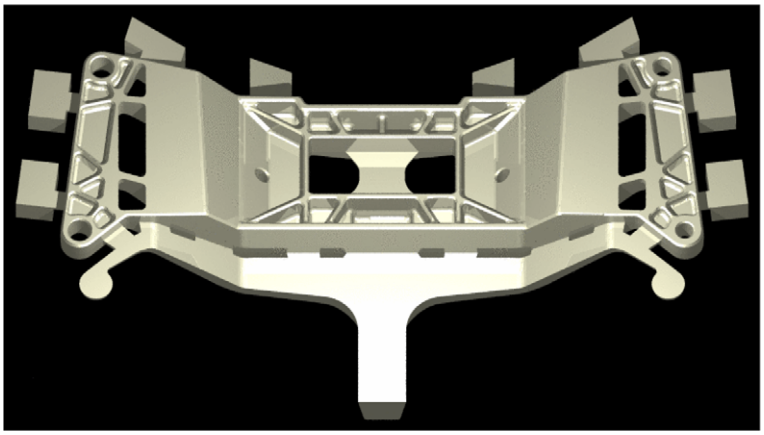

Fig. 13. Geometry of cross member.

At 60 ms there are four distinct unfilled areas. These are a large one directly in front of the gate, one near each of the side walls towards the end of the die and one along the centreline of the die directly adjacent to the end wall. At 80 ms, the back filling flow has closed the large void region adjacent to the gate, but the increasing viscosity of the solidifying metal makes it difficult for the fluid to flow into the last two remaining large scale voids. Eventually they do fill in this case, but this casting was close to being a cold shut.

4.2. Thermal validation by short shot comparison

Short shots are obtained by only partially filling a die cavity, generally by using a smaller shot volume. As the metal flows, it cools and starts to solidify. Eventually the metal stops moving and freezes in place, preserving significant amounts of information about the distribution of metal in the die and the nature of the flow. Fig. 8 shows a comparison of an experimental and simulated short shot for the cast aluminium coaster. The simulation is coloured by viscosity, with red[1] being a highly viscous fluid (almost solid). The predicted front profile is in very good agreement with the experiment. Note particularly the ability to predict the more restricted flow in the middle of the die due to the central island in the gate which acts as a significant thermal sink, leading to much more rapid solidification and less movement of the fluid front here.

5. Predicted filling of automotive parts

In the last two sections, we ascertain the accuracy of SPH in predicting the die filling process with and without heat transfer and solidification. Here, SPH simulations of the filling of a number of automotive components are presented. The filling patterns provide information on the order of fill and give guidance about potential sites of porosity formation. These can then be used as inputs for developing improved gate, runner and venting systems.

5.1. Servo piston

Fig. 9 shows the casting configuration for a four part servo piston. The shot sleeve leads through a converging right angle elbow runner into a chisel gate with a height of 3 mm. The piston head is a fairly simple almost axially symmetric top hat like structure. The base ranges from 0.4 to 0.7 cm in thickness and has a diameter of 11 cm. The diameter of the inner cylindrical structure is 6.4 cm and its height is 3.2 cm. There are three overflow vents on the far side of each piston. The particle size used for the simulation is 1.4 mm. Detailed validation of the SPH predicted fill pattern is presented in Section 3 for a single such piston by comparing to water analogue experiments and a matching MAGMAsoft solution.

[1] For interpretation of colour in figures, the reader is referred to the web version of this article.

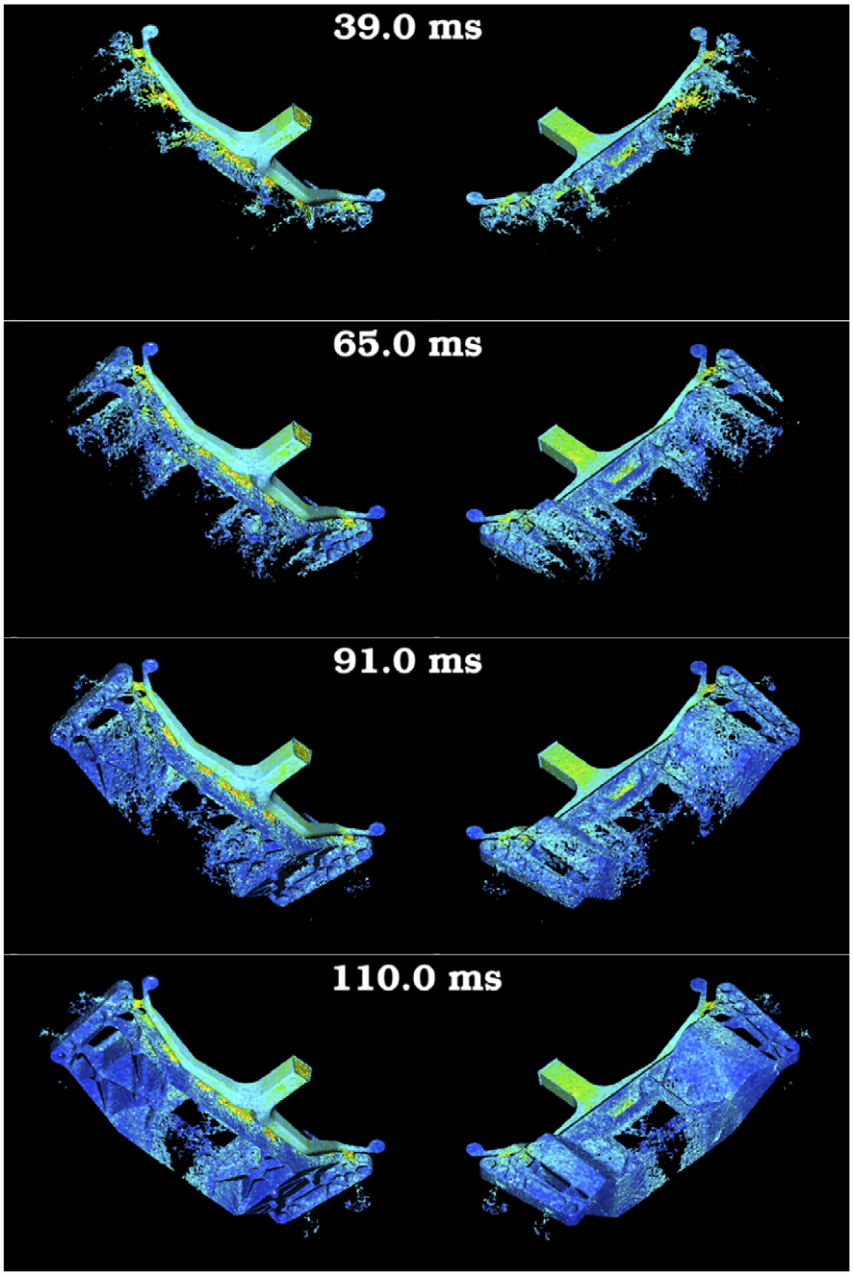

Fig. 14. Filling of cross member with fluid coloured by velocity.

Fig. 10 shows the progress of the fluid front which is coloured by speed, with the maximum being 50 m/s (red)[1] and the minimum being 0 m/s (dark blue). In the first frame, the fluid has just passed through the initial dog leg part of the runner and has split into the two main branches of the runner. Note that the flow separates from the curved side surfaces of the runner at each of the right angle bends and only occupies half the width of the runner on the gate side.

In the second frame, the fluid has passed through all four of the gates and has substantially back filled along the outsides of the runner back towards the dog leg feeder. The fluid passing through the gates rapidly moves into the four piston heads. The free surfaces are highly fragmented as the fluid splashes across each of the die

cavities. The pistons on either end are the first to fill due to the earlier back filling on the outsides of the runner leading to earlier pressurisation of the gates for the two outer dies.

The incoming stream hits the inside of the annular raised central sections of the dies and flows around the circular top edges of the pistons. The fluid rapidly reaches the opposite side and blocks the vents, leading to a strong back flow around the rim of the pistons and around the sides of the top hat. The last locations to fill are directly to either side of the gate. These observations were found to be consistent with the porosity map supplied by the manufacturer.

5.2. Rack and pinion steering column

Fig. 11 shows the die and Fig. 12 the filling of a component from a rack and pinion steering column. The two cylindrical structures are about 12 cm in length with an inner diameter of 1.25 cm. The simulation uses a particle size of 0.75 mm. The runner consists of two branches, one of which splits into two chisel gates and the other has a 180° annular gate. In this case the fluid attains a high velocity as it reaches the gate region. The first frame shows the fluid as it fragments and sprays out into the die cavity.

By 15 ms, fluid has filled the end of the die near the annular gate with a rapidly time varying honeycomb structure (which is not at all good for low porosity). The two small chisel gates both produce coherent sprays of small fluid fragments.

The fluid rapidly reaches the ends of the die and then back fills towards the gates. The volumetric rate of filling through the large gate at the left end of the die is much higher than through the chisel gates on the right, so the left cylindrical section fills much more rapidly. By 20 ms, significant amounts of fluid have flowed up into the vertical cylindrical projection at the junction of the two horizontal cylindrical sections. Some of the external cavity features on the die fill early, as some of the diverging fluid flow is able to flow into them, while others remain unfilled until the end. The last regions to fill in this component are the ones closest to the two gates, as seen in the last two frames of Fig. 12.

5.3. Structural cross member

Fig. 13 shows the die and Fig. 14 shows the filling of a cross bar support. This part is fairly topologically complex, consisting of several sections with strengthening ribs and various cut outs. There are nine gates distributed along the leading edge of the component and these are fed by a fairly conventional tangential runner system with shock absorbers at the ends. The gate height is 2.6 mm and the particle resolution used for this simulation was 1.7 mm. This die is interesting because of the partitioning created by the significant holes in the part and the high aspect ratio ribs.

The fluid sprays out from the gates along clear preferential pathways, leaving regions with long enduring voids on the sides of the central body where insufficient fluid can be supplied by this runner system. By 65 ms, the leading fluid reaches the far side of the die and much of the structure on the near side is substantially filled.

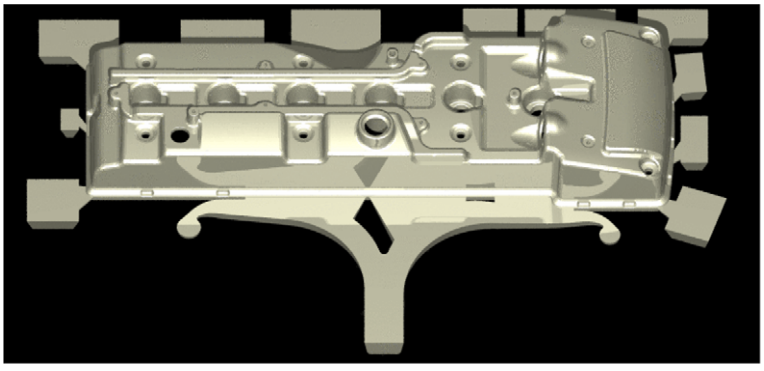

Fig. 15. Geometry of rocker cover.

By 91 ms, the entire die is mostly filled, but many areas still exhibit distinct moderate scale voidage. The final area to fill (shown in the last frame of Fig. 14) is in the middle of the far side of the die. This is a structurally critical location where porosity is highly undesirable. The simulation shows that despite the presence of a large central bridge which is intended to channel fluid into this region much earlier, this region is difficult to fill and could be subject to cold shuts, joining problems where the fronts of fluid meet from either side and also from trapped porosity.

5.4. Rocker cover

Fig. 15 shows the casting configuration for an engine rocker cover. It is about 750 mm × 250 mm in area. The section thickness is about 3 mm. A tangential runner system is skewed and feeds fluid through three long

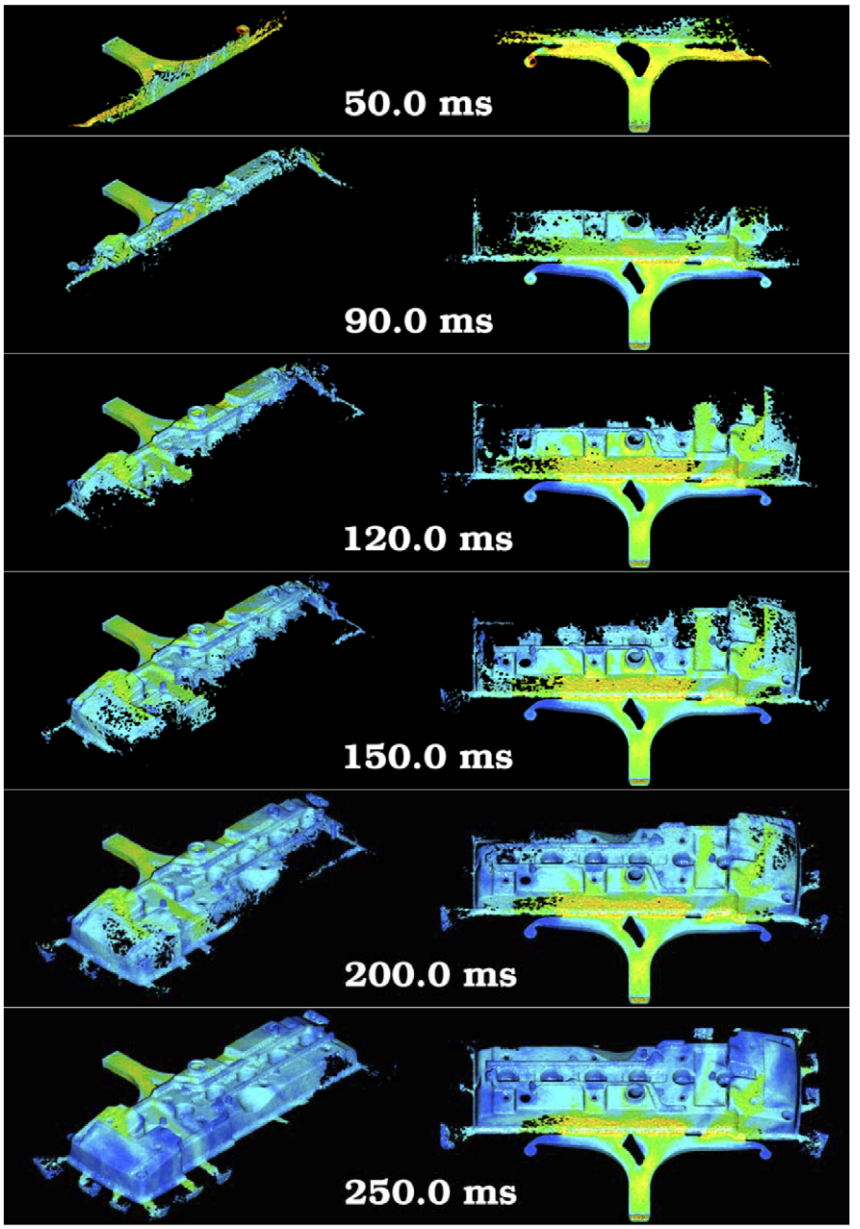

Fig. 16. Filling of rocker cover with fluid coloured by velocity.

gates with heights of 2 mm and gate speeds of around 12 m/s. The particle size used for this simulation was 1.25 mm. This is the largest part that has so far been simulated using SPH.

Fig. 16 shows the filling of this rocker cover. The long gates have a combined area that is similar to the runner cross sectional area, so the fluid does not accelerate much in passing through the gate regions in comparison with the previous castings presented. The lower gate speed results in somewhat reduced splashing and fragmentation of the fluid upon entry into the die (see frames at 50 and 90 ms).

The complex stepped contours of the die combine with the diverging of the flow from the gates leading to large long lived void areas (see filling state at 120 and 150 ms). This is essentially the result of the diverging flow from the gate being unable to maintain a uniform front, so fluid is not able to flow into the more protected regions of the die produced by the steps in the shape. Note that there is also clear evidence of preferential race tracking of fluid around the perimeter of the rocker cover (see frames at 150 and 200 ms).

By 250 ms, the die has substantially filled with critical voids remaining in just two locations, one just to the side of the gate (as seen in the fifth frame of Fig. 16) and one on the far side of the casting where recirculating fluid and the race track along the bottom edge has created a long lived roughly elliptical void (shown in the last frame of Fig. 16). Again these observations are consistent with observations made by the manufacturer.

6. Conclusions

To establish the accuracy of these types of SPH filling simulations, a comparison was made for a single servo piston between SPH and MAGMAsoft simulation results and a water analogue experiment. In the earlier stages of the simulations MAGMAsoft shows slightly better agreement with the experimental observations. However in the mid to late stages of the filling process, the SPH simulations show very good agreement with the fill pattern shown in the experiment with accurate predictions of the speed of propagation of fluid fronts and the times at which voids are trapped. In contrast, the MAGMAsoft simulation rapidly diverges from the experimental flow, with significant errors predicted in the strengths of the base plate jets and of the fluid flow around the sides of the central raised cylindrical section. The SPH predictions of fill pattern and regions of possible voids in the die show good to excellent agreement with the experimental observations for this die.

To validate SPH simulation of die filling which is fully coupled to heat transfer and solidification, short shots of a simple coaster with tangential runners was used. This highlighted the additional complexities that heat transfer and solidification introduce in the die filling process and particularly the possibility of predicting cold shuts.

The filling of several automotive components, ranging from a simple servo piston to a full engine rocker cover, by the HPDC process were simulated using SPH. The detail in the filling predictions is very high and the last locations to fill correlate well with porosity/voidage observations made by manufacturers of these components.

This study demonstrates the ability of SPH to produce good quality and reasonably accurate solutions at quite low resolutions, particularly of the fragmenting and sub-dividing parts of the flow. It potentially offers the die-casting industry a new way of making better predictions of the HPDC process that could lead to thinner shell thicknesses (i.e. lighter and cheaper parts), faster cycle times, less scrap and lower reject rates and particularly faster development times for new dies.

Acknowledgement

This work was partially funded by the Cooperative Research Centre for Cast Metals Manufacturing (CAST).

References

[1] MAGMA GMBH, 2000. MAGMAsoft Release 4.0.
[2] J.J. Monaghan, Smoothed particle hydrodynamics, Ann. Rev. Astron. Astrophys. 30 (1992) 543–574.
[3] J.J. Monaghan, R.A.F. Cas, A. Kos, M. Hallworth, Gravity currents descending a ramp in a stratified tank, J. Fluid Mech. 379 (1999) 39–70.

[4] J.J. Monaghan, A. Kos, Solitary waves on a Cretan beach, J. Waterways, Ports, Coastal Ocean Eng. 125 (1999) 145–154.
[5] J.J. Monaghan, A. Kos, Scott Russell's wave generator, Phys. Fluids A 12 (2000) 622–630.
[6] J.P. Morris, P.J. Fox, Y. Zhu, Modeling low Reynolds number incompressible flows using SPH, J. Comput. Phys. 136 (1997) 214–226.
[7] S.J. Cummins, M. Rudman, An SPH projection method, J. Comput. Phys. 152 (1999) 584–607.
[8] H. Takeda, S.M. Miyama, M. Sekiya, Numerical simulation of viscous flow by smoothed particle hydrodynamics, Prog. Theor. Phys. 92 (1994) 939–960.
[9] J.W. Swegle, S.W. Attaway, On the feasibility of using smoothed particle hydrodynamic for underwater explosion calculations, Comput. Mech. 17 (1995) 151.
[10] J. Hultman, D. Kallander, An SPH code for galaxy formation problems: presentation of the code, Astron. Astrophys. 324 (1997) 534–548.
[11] P.W. Cleary, J.J. Monaghan, Conduction modelling using smoothed particle hydrodynamics, J. Comput. Phys. 148 (1999) 227–264.
[12] P.W. Cleary, Modelling confined multi-material heat and mass flows using SPH, Appl. Math. Model. 22 (1998) 981–993.
[13] P.W. Cleary, J. Ha, J. Mooney, V. Ahuja, Effect of heat transfer and solidification on high pressure die casting, in: Proc. 13th Australasian Fluid Mechanics Conference, Melbourne, Australia, 1998, pp. 679–682.
[14] P.W. Cleary, J. Ha, V. Ahuja, High pressure die casting simulation using smoothed particle hydrodynamics, Int. J. Cast Metals Res. 12 (2000) 335–355.
[15] J. Ha, P.W. Cleary, Comparison of SPH simulations of high pressure die casting with the experiments and VOF simulations of Schmid and Klein, Int. J. Cast Metals Res. 12 (2000) 409–418.
[16] J. Ha, P.W. Cleary, V. Alguine, T. Nguyen, Simulation of die filling in gravity die casting using SPH and MAGMAsoft, in: Proc. 2nd Int. Conf. on CFD in Minerals & Process Industries, Melbourne, Australia, 1999, pp. 423–428.
[17] J.J. Monaghan, Simulating free surface flows with SPH, J. Comput. Phys. 110 (1994) 399–406.